Impedance of SOFC electrodes: A review and a comprehensive case study on the impedance of LSM:YSZ cathodes

Nielsen, Jimmi; Hjelm, Johan

Published in:
Electrochimica Acta

Link to article, DOI:
10.1016/j.electacta.2013.10.053

Publication date:
2014

Document Version
Publisher's PDF, also known as Version of record

Electrochimica Acta 115 (2014) 31–45

Contents lists available at ScienceDirect

Electrochimica Acta

journal homepage: www.elsevier.com/locate/electacta

Impedance of SOFC electrodes: A review and a comprehensive case study on the impedance of LSM:YSZ cathodes☆

Jimmi Nielsen*, Johan Hjelm

Department of Energy Conversion and Storage, Technical University of Denmark, Frederiksborgvej 399, Roskilde DK-4000, Denmark

ARTICLE INFO

Article history:
Received 24 May 2013
Received in revised form 7 October 2013
Accepted 7 October 2013
Available online 24 October 2013

Keywords:
SOFC
Impedance
LSM:YSZ
Cathodes
Anodes

ABSTRACT

It was shown through a comprehensive impedance spectroscopy study that the impedance of the classic composite LSM:YSZ (lanthanum strontium manganite and yttria stabilized zirconia) solid oxide fuel cell (SOFC) cathode can be described well with porous electrode theory. Furthermore, it was illustrated through a literature review on SOFC electrodes that porous electrode theory not only describes the classic LSM:YSZ SOFC cathode well, but SOFC electrodes in general. The extensive impedance spectroscopy study of LSM:YSZ cathodes consisted of measurements on cathodes with three different sintering temperatures and hence different microstructures and varying degrees of LSM/YSZ solid state interactions. LSM based composite cathodes, where YSZ was replaced with CGO was also studied in order to acquire further knowledge on the chemical compatibility between LSM and YSZ. All impedance measurements were acquired in the very broad temperature range of 200–900 °C for complete elucidation of the impedance. All impedance spectra were analyzed in terms of porous electrode theory. Physical materials parameters were extracted from the analysis, which were in excellent accordance with literature values. Valuable insight about the dissolution of Mn in the cathode composite material YSZ during preparation was furthermore provided along with valuable engineering characteristics such as the electrochemical utilization thickness. From the combined impedance study and literature review, it is clear, that porous electrode theory is the most suitable framework for any type of porous composite SOFC electrode evaluation.

1. Introduction

Solid oxide fuel cells (SOFCs) have been subject to extensive research in the past 20–40 years. The key challenge is to achieve a competitive balance between cost, efficiency and durability. Thus, for improvement and optimization it is important to understand the losses and the degradation mechanisms within SOFCs. Electrochemical impedance spectroscopy (EIS) has proven itself as a powerful technique for breaking down the losses within a SOFC, but also to provide insight into which component and/or process primarily degrade during operation. Despite the significant body of research conducted in this area, the impedance of SOFC electrodes has primarily been evaluated by a fairly primitive approach consisting of a series of suppressed semi circles (see e.g. reviews [1–3]). Each suppressed semicircle is then usually ascribed to a specific reaction or process. However, such an approach is often not a correct approximation since processes can be coupled. Examples of coupled processes include the Finite-Length-Warburg (FLW) impedance element describing diffusion followed by reaction [4], gas diffusion coupled with gas conversion in e.g. SOFC anodes [5], the Gerischer impedance element describing a coupling between diffusion and reaction [6] and the de Levie response of porous electrode theory describing the coupling between ionic conduction in an electrolyte and a reaction [7]. For maximisation of the active reaction area and hence a lowering of the polarization resistance, SOFC electrodes consists today of interpenetrating ionically and electronically conducting networks. This can be achieved by the use of mixed ionic electronic conductor (MIEC) materials or composite electrodes where one material is a good electronic conductor and the other material a good oxide ion conductor. Similar concepts with the electrode consisting both of an electronically and an ionically conducting network can be found in many areas of electrochemistry. The impedance response of such systems can be described by porous electrode theory (PET). Examples of areas, which successfully have made use of PET include porous electrodes in aqueous solutions [7,8], super capacitors [9,10], batteries [11–13], conducting polymer electrodes [14–17] and polymer fuel cell membrane electrode assemblies [18,19].

Despite a short proceeding paper in 1997 on LSM:YSZ cathodes [20], it is only very recently that the PET de Levie EIS model has

* Corresponding author. Tel.: +4546775626; fax: +45 4677 5858.
E-mail address: jini@dtu.dk (J. Nielsen).

0013-4686/$ – see front matter © 2013 The Authors. Published by Elsevier Ltd. All rights reserved.
http://dx.doi.org/10.1016/j.electacta.2013.10.053

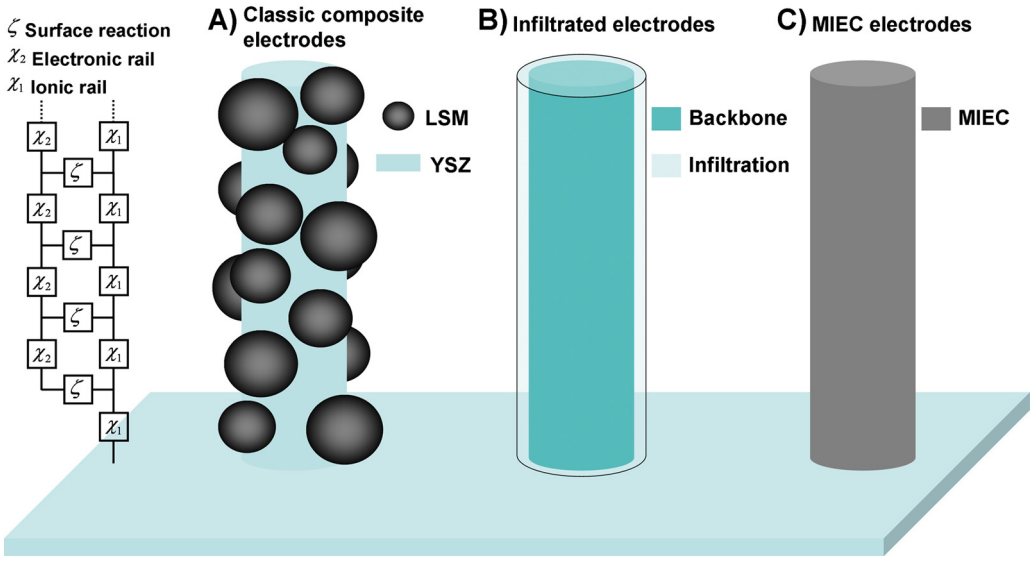

Fig. 1. Transmission line describing the various SOFC electrode models. (A) Model of classic composite electrodes. In this particular case the LSM:YSZ composite cathode. (B) Model of an infiltrated electrode. (C) Model of a mixed ionic electronic conductor (MIEC) material based cathode.

been employed for SOFC electrodes. Sonn et al. have made use of the transmission line in Fig. 1 to describe the impedance of the SOFC Ni:YSZ cermet anode [21]. However, they referred to the model as originating from composite polymer electrodes. Furthermore, even though the goodness of fit as χ^2 was provided with the transmission line model equivalent to the PET de Levie EIS model, the actual fits were not shown. Nonetheless, the parameters from fitting with the model made good physical sense. Recently, the author et al. of the present study employed the PET de Levie EIS model on a Ni:CGO infiltrated electronically conducting FeCr backbone for metal supported SOFC (MS-SOFC), where good fits were obtained over a large temperature span and valuable information could be extracted [22].

The aim of the present combined impedance study and review is to illustrate the applicability and the fundamental insight that the PET can provide in the understanding of SOFC electrodes. The study consists of a comprehensive study on the electrochemical impedance of the classic and technologically relevant composite LSM:YSZ cathode. The study includes measurements on LSM:YSZ cathodes on YSZ electrolytes sintered at three different temperatures, which result in different microstructures. Furthermore, measurements have been performed on a LSM:YSZ cathode on a CGO electrolyte and on a LSM:CGO cathode on a CGO electrolyte. The impedance of all cathode/electrolyte assemblies have been measured in the broad temperature range of 200–900 °C. The different material combinations were investigated in order to provide insight into the role of the chemical compatibility of LSM and YSZ. It is e.g. well known that LSM and YSZ may react and form resistive secondary phases consisting of zirconates ($La_2Sr_2ZrO_7$ and $SrZrO_3$) [2,23–26]. All the impedance responses of the different cathode/electrolyte assemblies have been studied on the basis of the PET de Levie model. The second aim of the present paper is to review some of the reported impedance observations and corresponding interpretations in the literature in the light of PET to illustrate that PET is an excellent and very fruitful description of SOFC electrodes. At last it is discussed how various dispersion effects can distort the impedance predicted by the PET.

2. Theory

The structure of a porous electrode immersed in, and filled with, a liquid electrolyte is in porous electrode theory (PET) modelled as cylindrical pores containing the electrolyte, while the pore wall corresponds to the surface of the solid electronically conducting electrode. For detailed and further knowledge on classic PET the reader is referred to the recent review by Lasia [8]. In the case of composite SOFC electrodes a similar situation exists with (bi-continuous) percolated networks of electronically and ionically conducting particles. The structure of SOFC composite electrodes e.g. LSM:YSZ can be modelled as YSZ columns surrounded by the LSM electrocatalyst as illustrated in Fig. 1A. The classic composite Ni:YSZ cermet SOFC anode can be modelled in a similar fashion by replacing LSM with Ni [21]. For infiltrated SOFC electrodes a backbone is covered with infiltrated material as illustrated in Fig. 1B. The backbone is either an oxide ion conductor or an electronic conductor, which is infiltrated by an appropriate material catalyst so that an electrode with both an electronically and an ionically conducting network is obtained. For MIEC cathodes the ionically and electronically conducting networks are contained within the same material and can therefore be modelled simply as columns as illustrated in Fig. 1C. The coupling between the impedance of the percolated conducting networks χ_1 and χ_2 and the impedance of the electrochemical reaction ζ can be described by the general transmission line depicted to the left in Fig. 1. The solution of the general transmission line is given by [16,17]:

$$Z = \frac{\chi_1\chi_2}{\chi_1+\chi_2}\left(L + \frac{2\lambda}{\sinh\left(L/\lambda\right)}\right) + \lambda\frac{\chi_1^2+\chi_2^2}{\chi_1+\chi_2}\coth\left(\frac{L}{\lambda}\right) \quad (1)$$

with

$$\lambda = \sqrt{\frac{\zeta}{\chi_1+\chi_2}} \quad (2)$$

Here L is the thickness of the electrode and λ is the characteristic AC penetration thickness, the latter of which is equivalent to the electrochemical utilization thickness of the electrode. The tortuosity τ of the conducting electrode pathway is the ratio between the length of the conducting pathway δ and the thickness L of the electrode $\tau = \delta/L$. The thickness is usually determined from cross sectional micrographs of the electrode. Eq. (1) represents the impedance (in Ω) of a single column shown in Fig. 1, but in principle the porous electrode consists of n columns pr. area. However, it is difficult to determine the exact number of columns per area in the porous electrode. A much easier and equivalently informative approach is to consider the porous electrode effectively as one

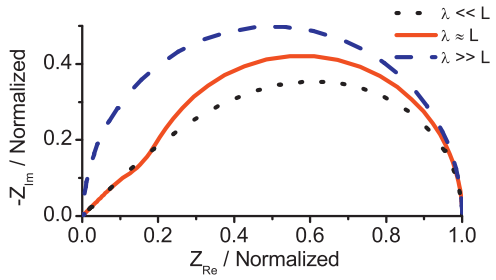

Fig. 2. Possible impedance spectrum shapes for $\alpha_r = 1$ in Eq. (5) of the porous electrode theory de Levie response.

column pr. area. This enables direct application of Eq. (1). For practical composite electrodes the electronic conductivity is much higher than the ionic conductivity $\chi_2 \ll \chi_1$, which results in simplification of Eq. (1) to:

$$Z = \lambda\chi_1 \coth\left(\frac{L}{\lambda}\right),$$

with

$$\lambda = \sqrt{\frac{\zeta}{\chi_1}} \tag{3}$$

The transport of oxide ions can be modelled as a resistance per unit length (in Ω/cm):

$$\chi_1 = r_c \tag{4}$$

Finally the impedance of the surface reaction ζ (in Ω cm) may be modelled as a simple parallel combination between a resistor r_r and a constant phase element q_r (CPE):

$$\zeta = \frac{r_r}{1 + r_r q_r (j\omega)^{\alpha_r}} \tag{5}$$

The unit of the impedance ζ is Ω cm because it is the area specific impedance of the column surface (in Ω cm^2) divided by the perimeter of the column. The case with assumptions (4) and (5) is in the following referred to as PET de Levie, since it is similar to original PET response derived by de Levie [7]. In the given interpretation it is of cause important to mention that for the LSM:YSZ cathode modelling in Fig. 1A, with the reaction taking place at the three-phase-boundary (TPB) zone, r_r in Eq. (5) represents a volumetric average value. The same applies to the similar modelling of the classic Ni:YSZ cermet SOFC anode. The possible PET de Levie impedance shapes for $\alpha_r = 1$ in Eq. (5), depending on the electrode utilization thickness λ relative to the electrode thickness, are depicted in Fig. 2. Further discussions on the validity of the model can be found in Section 7 discussing PET dispersion effects.

3. Experimental

3.1. Preparation of symmetrical cells

The symmetrical cells with $(La_{0.8}Sr_{0.2})_{0.98}MnO_{3-\delta}/Zr_{0.92}Y_{0.08}O_{1.96}$ (LSM:YSZ) cathodes were prepared using commercial available screen printing paste from ESL ElectroScience. The LSM:CGO cathode screen printing pastes were prepared in house by mixing 50:50 wt% $(La_{0.8}Sr_{0.2})_{0.95}MnO_{3-\delta}$ and $Gd_{0.8}Ce_{0.2}O_{1.9}$. Suspensions (inks) of the raw powders were produced using a solvent, a binder and a surfactant, and mixing and milling was carried out using a planetary ball mill. The cathode inks were screen printed onto both sides of either an YSZ or a CGO substrate. The used approximately 150 μm thick YSZ substrates were prepared in house by tape casting, while the used approximately 250 μm thick CGO substrates were commercially available (Kerafol, Germany). These cells, containing green ceramic layers, were laser cut to $6 \times 6\,mm^2$ samples, sintered at the desired temperatures 980 °C, 1080 °C and 1180 °C and later used in the symmetrical cell tests.

3.2. Electrochemical measurements

The sintered $6 \times 6\,mm^2$ symmetrical cells were painted with Pt paste on both sides to form current collecting layers. The painted cells were subsequently sintered at 920 °C for 2 h and were hereafter sandwiched in between fine Pt meshes in the test setup. The measurements were conducted in specially designed rigs, which have been constructed to allow simultaneous testing of four symmetric cells, with fully automated changes of testing conditions, such as temperature and gas composition. The cells were characterized by electrochemical impedance spectroscopy (EIS) at open circuit voltage (OCV) in air and oxygen atmospheres in the temperature range 200–900 °C with EIS acquisition at intervals of 50 °C. The impedance spectra were obtained using a Solartron 1260 FRA in the frequency range 1 MHz–1 mHz. For the impedance spectra recorded at high temperature the low frequency limit was higher than 1 mHz in order to reduce the recording time. The EIS perturbation amplitude was 30 mV RMS in all cases. That linearity was fulfilled was checked by polarization curves of the studied symmetrical cells. The acquired EIS data were corrected for inductance from wires etc. by using the Kramers–Kronig relation. The impedance data were analyzed in a custom MATLAB program with model fitting using the Levenberg–Marquardt complex non-linear least square (CNLS) algorithm. For comparison of CPE Q elements with the impedance $Z = 1/Q(j\omega)^{\alpha}$ the following equivalent capacitance C_w was used according to [27]:

$$C_w = \left(R^{1-\alpha}Q\right)^{1/\alpha} \tag{6}$$

The used notation for EIS equivalent circuits is that of Boukamp [28]. For elements such as the PET de Levie model and the Finite-Length-Warburg, the abbreviations PET and FLW were used, respectively.

3.3. Microscopy

The microstructure of polished cross-sections of the symmetrical cell samples were characterized by scanning electron microscopy (SEM). These samples were prepared by vacuum embedding the samples in Struers epoxy resin (Epofix); ground using SiC paper; polished using 6 μm, 3 μm and 1 μm diamond paste, and then carbon coated to eliminate surface charging. The samples were examined using a Zeiss Supra 35 equipped with a field emission gun (FEG).

4. Results on LSM based cathodes

The impedance of LSM based SOFC composite cathodes are in the following sections systematically and thoroughly studied in detail. The effect of sintering temperature was studied on YSZ based LSM composite cathodes on YSZ electrolytes (LSM:YSZ/YSZ). This was done in order to acquire information about possible solid state reactions leading to the formation of secondary zirconate phases ($La_2Sr_2ZrO_7$ and $SrZrO_3$). Furthermore these studies are compared with similar impedance studies on LSM:YSZ cathodes on CGO electrolytes (LSM:YSZ/CGO) and LSM:CGO cathodes on CGO electrolytes (LSM:CGO/CGO). All studies were performed on polycrystalline electrolytes, which not only correspond well to the technologically relevant situation, but it is also most similar to the majority of the studies reported in the literature. Hence, comparison of results in the present study with literature can be performed easier and more directly. The use of polycrystalline

Table 1
Summary of (RQ) arc equivalent capacitances C_w for the resolved arcs in the 300 °C EIS spectrum in Figs. 3 and 5–6 and the 200 °C EIS spectrum in Figs. 7–8. The extracted activation energies for the r_c and r_r parameters from the PET de Levie fitting is also summarized.

Interpretation	Grain interior	Grain boundary	Electrode		
Type of assembly	Arc I(C_w F/cm^2)	Arc II(C_w F/cm^2)	Arc III(C_w F/cm^2)	E_a (r_c)(kJ/mol)	E_a (r_r)(kJ/mol)
LSM:YSZ/YSZ sintered at 980 °C	8×10^{-10}	1×10^{-6}	–	92	158
LSM:YSZ/YSZ sintered at 1080 °C	7×10^{-10}	2×10^{-6}	1×10^{-5}	90	161
LSM:YSZ/YSZ sintered at 1180 °C	7×10^{-10}	8×10^{-7}	2×10^{-5}	114	155
LSM:YSZ/CGO sintered at 1180 °C	5×10^{-10}	3×10^{-8}	4×10^{-5}	114	149
LSM:CGO/CGO sintered at 1180 °C	4×10^{-10}	3×10^{-7}	–	86	114

electrolytes implies that responses from the YSZ grain interior (grain bulk), and the YSZ grain boundaries are present if the complete impedance spectrum is acquired. Acquisition of the complete EIS spectrum should provide a less unambiguous interpretation of the impedance. This is achieved by studying the impedance of all the cathode/electrolyte assemblies in the very broad temperature range of 200–900 °C with impedance acquisition at intervals of 50 °C, and by using a sufficiently wide frequency range. Selected

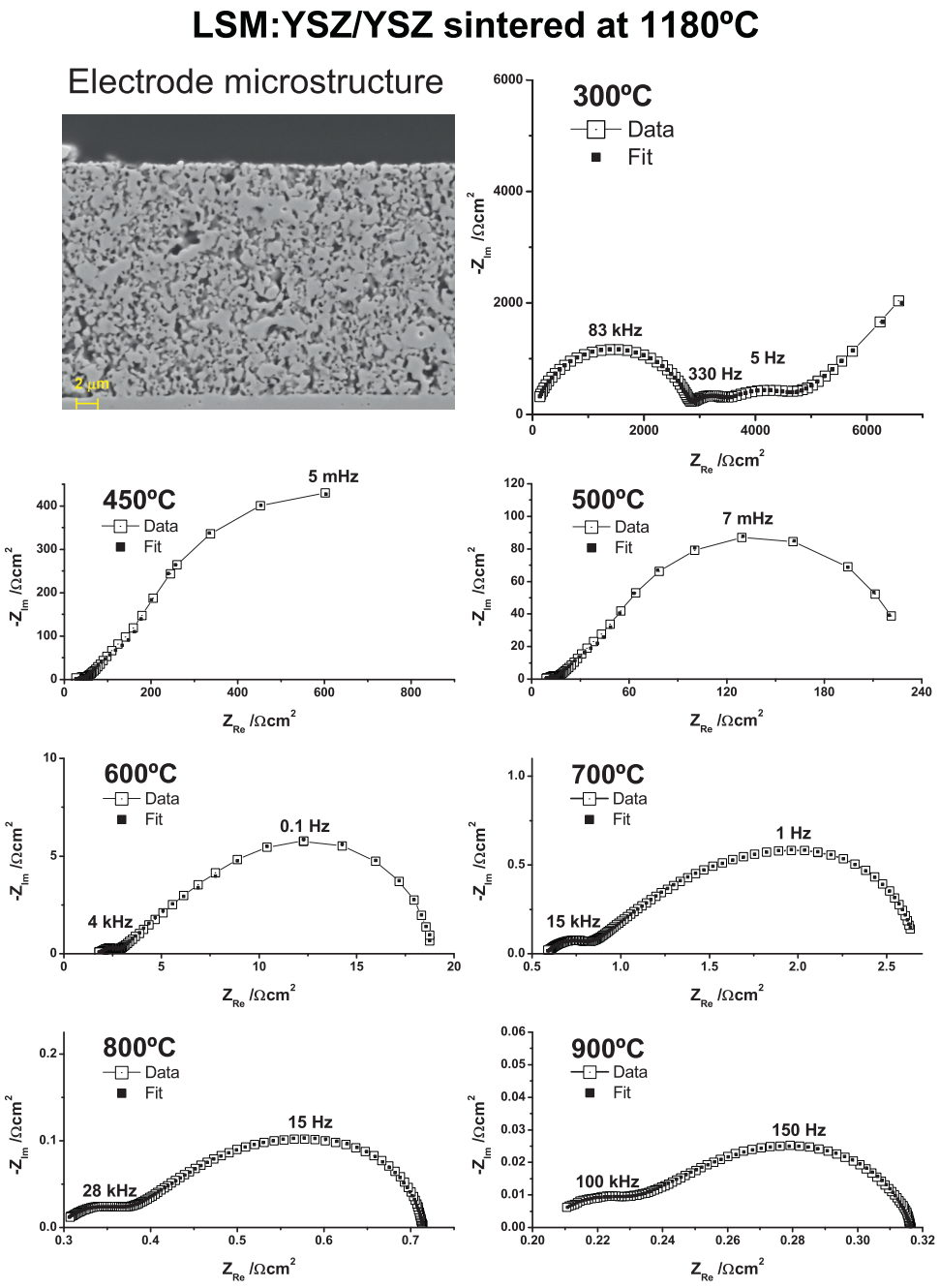

Fig. 3. Impedance spectra in the temperature range 300–900 °C of a LSM:YSZ composite cathode on a YSZ electrolyte sintered at 1180 °C. The impedance has been fitted with the equivalent circuit $(RQ)_1$–$(RQ)_2$–$(RQ)_3$–PET at low temperatures and $R_s(RQ)_3$–PET at high temperatures.

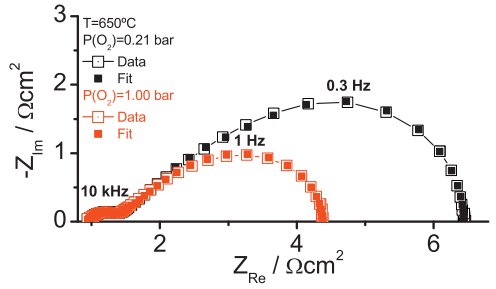

Fig. 4. Impedance spectra of a LSM:YSZ composite cathode on a YSZ electrolyte in air and an oxygen atmosphere at 650 °C, respectively. The symmetrical cell is sintered at 1180 °C. The change in impedance can be accounted for fitting wise solely by a change in PET de Levie electrochemical surface reaction r_r.

results from the various cathode/electrolyte assemblies are summarized in Table 1 and discussed in detail in Section 5.

4.1. Results on LSM:YSZ/YSZ cathodes sintered at 1180 °C

Fig. 3 shows the impedance in the temperature range 300–900 °C of symmetrical cells with LSM:YSZ cathodes and an YSZ electrolyte sintered at 1180 °C. The low frequency arc is the PET de Levie impedance response, which at high temperatures has the characteristic skewed semicircle shape (case $L \gg \lambda$ in Fig. 2). The PET de Levie impedance response changes around 500 °C into a shape consisting of 45° slope at high frequencies (the angle depends on the suppression factor α of the CPE in Eq. (5)) and a suppressed semicircle at low frequencies (case $L \sim \lambda$ in Fig. 2). At lower temperatures the PET de Levie EIS shape is expected to change completely into a suppressed semicircle (case $L \ll \lambda$ in Fig. 2). However, the PET de Levie suppressed semicircle is located at very low frequencies, which makes it experimentally difficult to measure. At high temperatures the EIS response seems to consist of a high frequency (RQ) arc followed by the PET de Levie response. At 300 °C it is possible to resolve the whole high-frequency (HF) region from which three (RQ) arcs are clearly distinguished followed by the PET de Levie response. The impedance has been fitted to the equivalent circuit $(RQ)_1$–$(RQ)_2$–$(RQ)_3$–PET at low temperatures and $(RQ)_3$–PET at high temperatures. The used (RQ) arcs primarily originating from the electrolyte are discussed in detail in Section 5.1. As can be seen from Fig. 3 good fits are obtained. However, a slight deviation is observable in the PET transition zone where the response goes from a straight line to a suppressed semicircle in the $T = 450$ °C and $T = 500$ °C spectra (case $L \sim \lambda$ in Fig. 2). This may be explained by a distributed diffusion pathway length L equivalent to a distribution in column height in Fig. 1 as is discussed further in Section 7 concerning dispersion effects. From the fits with the PET de Levie EIS model, activation energies for r_c and r_r can be extracted as shown in Fig. 9. The result is activation energies of 114 kJ/mol and 155 kJ/mol, respectively. In Fig. 4 the effect on impedance is shown of changing the atmosphere from air to pure oxygen. As expected from the PET de Levie EIS model the change in oxygen partial pressure in Fig. 4 can be accounted for solely by a change in the impedance of the surface reaction ζ in Eq. (5).

4.2. Results on LSM:YSZ/YSZ cathodes sintered at 1080 °C

Fig. 5 shows the impedance in the temperature range 300–900 °C of symmetrical cells with LSM:YSZ cathodes and an YSZ electrolyte sintered at 1080 °C. Unlike the LSM:YSZ cathodes sintered at 1180 °C in Fig. 3, the LSM:YSZ cathodes sintered at 1080 °C do not go into the Finite PET de Levie case with $L \ll \lambda$. This is due to the finer microstructure as a consequence of the lower sintering temperature, which results in a larger LSM/YSZ TPB length within the porous electrode, and thus a lower reaction resistance r_r and as a result also a smaller cathode utilization thickness λ. From the spectrum recorded at 300 °C only two clearly resolved (RQ) arcs followed by the PET de Levie EIS response are observed. This is unlike the cathode sintered at 1180 °C in Fig. 5, where three clearly resolved (RQ) arcs prior to the PET de Levie response were observed. However, upon fitting of the spectra it is clear that it is necessary to include three (RQ) arcs prior to the PET de Levie response in Fig. 5 to account for the impedance. Thus, the low temperature spectra in Fig. 5 have been fitted with the equivalent circuit $(RQ)_1$–$(RQ)_2$–$(RQ)_3$–PET, while the high temperature spectra >800 °C has been fitted with the equivalent circuit $(RQ)_3$–PET–FLW. For the high temperature spectra a Finite-Length-Warburg impedance element has been added to account for the oxygen gas diffusion, which is resolved for well performing cathodes. This is in complete accordance with previous reports on well performing cathodes [29]. The activation energies for the PET de Levie parameters r_c and r_r can be seen in Fig. 9 to be 90 kJ/mol and 161 kJ/mol, respectively.

4.3. Results on LSM:YSZ/YSZ cathodes sintered at 980 °C

Fig. 6 shows the impedance in the temperature range 300–900 °C of symmetrical cells with LSM:YSZ cathodes and an YSZ electrolyte sintered at 980 °C. The same conclusions as for the 1080 °C sintered cathodes presented in Section 4.2 and shown in Fig. 5 can be made. However, in the fitting of the spectra it is only necessary with two (RQ) combinations prior to the PET de Levie response. Thus, the low temperature spectra in Fig. 6 has been fitted with the equivalent circuit $(RQ)_1$–$(RQ)_2$–PET, while the high temperature spectra has been fitted with the equivalent circuit $(RQ)_2$–PET–FLW. The activation energies for the PET de Levie parameters, r_c and r_r, can be seen in Fig. 9 to be 92 kJ/mol and 158 kJ/mol, respectively.

4.4. Results on LSM:YSZ/CGO cathodes sintered at 1180 °C

Fig. 7 shows the impedance in the temperature range 200–900 °C of symmetrical cells with LSM:YSZ cathodes and a CGO electrolyte sintered at 1180 °C. Unlike the cathodes on YSZ electrolyte it is necessary to go to 200 °C in order to resolve the whole EIS spectrum. At 200 °C a small HF arc can be resolved. The capacitance C_w of the HF arc is 5×10^{-10} F/cm^2, which is on the same order of magnitude as the capacitance of the HF arc of the cathodes on YSZ electrolytes in Sections 4.1–4.3. This is summarized in Table 1 and discussed further in Section 5. The capacitance of the HF arc is ascribed the bulk capacitance of the electrolyte materials. Hence, all impedance contributions have been accounted for. The impedance spectra in Fig. 7 in temperature range 300–700 °C has been fitted with the equivalent circuit $(RQ)_2$–$(RQ)_3$–PET, while the spectra above 700 °C has been fitted with the equivalent circuit $(RQ)_3$–PET. The activation energies for the PET de Levie parameters r_c and r_r can be seen in Fig. 9 to be 114 kJ/mol and 149 kJ/mol, respectively.

4.5. Results on LSM:CGO/CGO cathodes sintered at 1180 °C

Fig. 8 shows the impedance of symmetrical cells with LSM:CGO cathodes sintered onto a CGO electrolyte at 1180 °C in the temperature range 200–900 °C. As in the measurements in Section 4.4, it is necessary to go to 200 °C to resolve the electrolyte (CGO) bulk response. In contrast to the LSM:YSZ/CGO measurements in Section 4.4 there is one (RQ) arc less. Thus, all impedance spectra in Fig. 8 recorded above 300 °C has been fitted with the equivalent circuit $(RQ)_2$–PET. The activation energies for the PET de Levie parameters

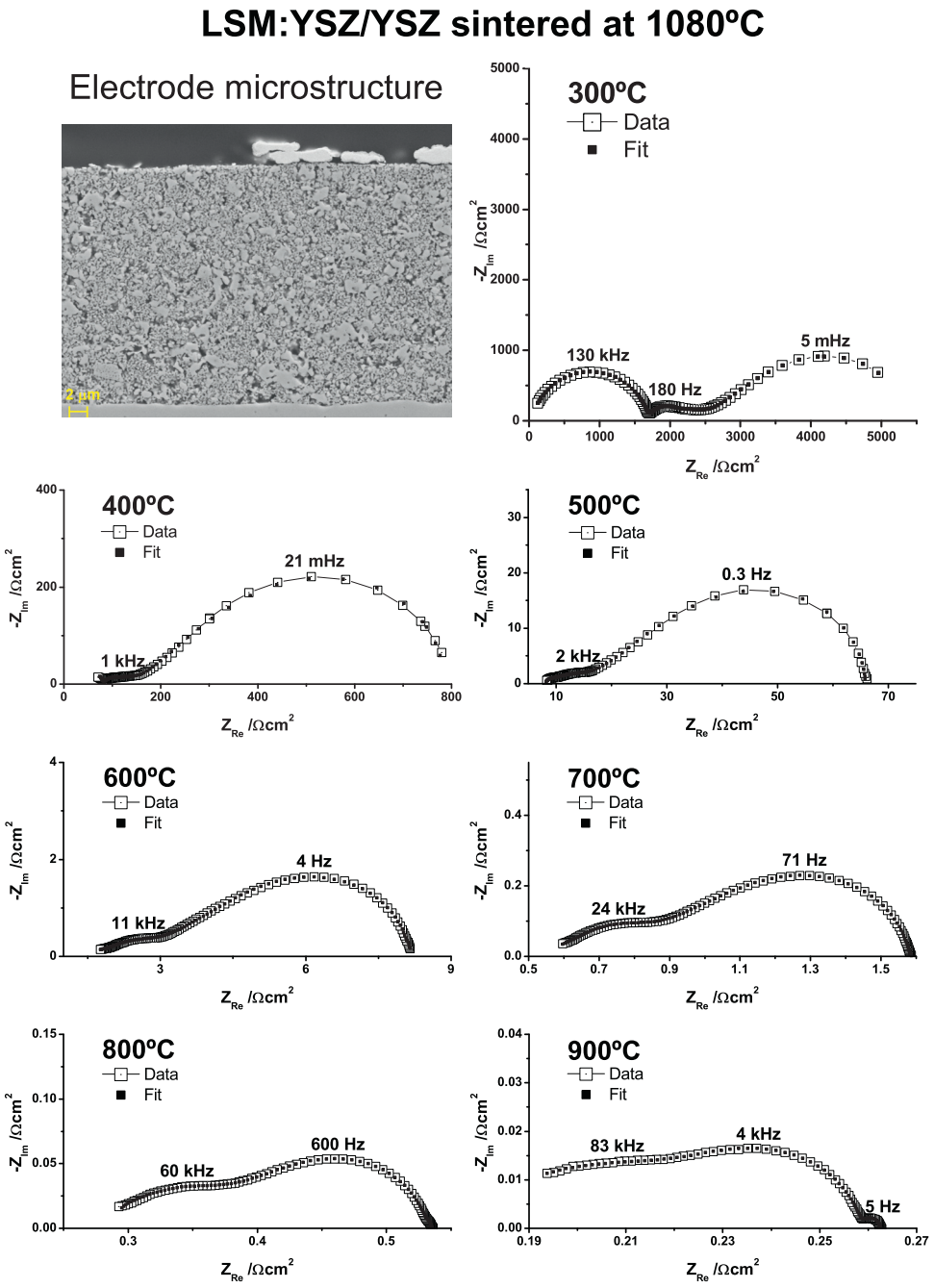

Fig. 5. Impedance spectra in the temperature range 300–900 °C of a LSM:YSZ composite cathode on a YSZ electrolyte sintered at 1080 °C. The low temperature spectra have been fitted with the equivalent circuit $(RQ)_1$–$(RQ)_2$–$(RQ)_3$–PET, while the high temperature spectra >800 °C has been fitted with the equivalent circuit $R_s(RQ)_3$–PET–FLW.

r_c and r_r can be seen in Fig. 9 to be 86 kJ/mol and 114 kJ/mol, respectively.

5. Discussion of results

5.1. Capacitance values and EIS arc assignment

The relative permittivity ε' of YSZ has been estimated to be 30 in [30]. Using this it is possible to calculate the expected area specific bulk capacitance of the used 150 μm thick YSZ electrolyte according to Eq. (7):

$$C = \frac{\varepsilon' e_0}{l} \quad (7)$$

where e_0 is the permittivity of free space (8.854×10^{-14} F/cm), l is the thickness of the sample. Doing the calculation, one arrives at an area specific capacitance of 2×10^{-10} F/cm^2 in good accordance with experimentally found C_w values of arc I in Table 1. Arc I represents the electrolyte bulk, or equivalently the grain interior (GI) capacitance, coupled with the YSZ bulk conduction resistance. Arc II is the grain boundary (GB) capacitance coupled with the grain boundary conduction resistance. In Table 1 the C_w values for arc II is around 10^{-7}–10^{-6} F/cm^2 for the used YSZ electrolyte, while for the CGO electrolyte the C_w capacitance is around 10^{-8}–10^{-7} F/cm^2. These values lie within the grain boundary capacitance range reported for YSZ and CGO in [31,32], where the effect of preparation and sintering temperature has been studied. From the results

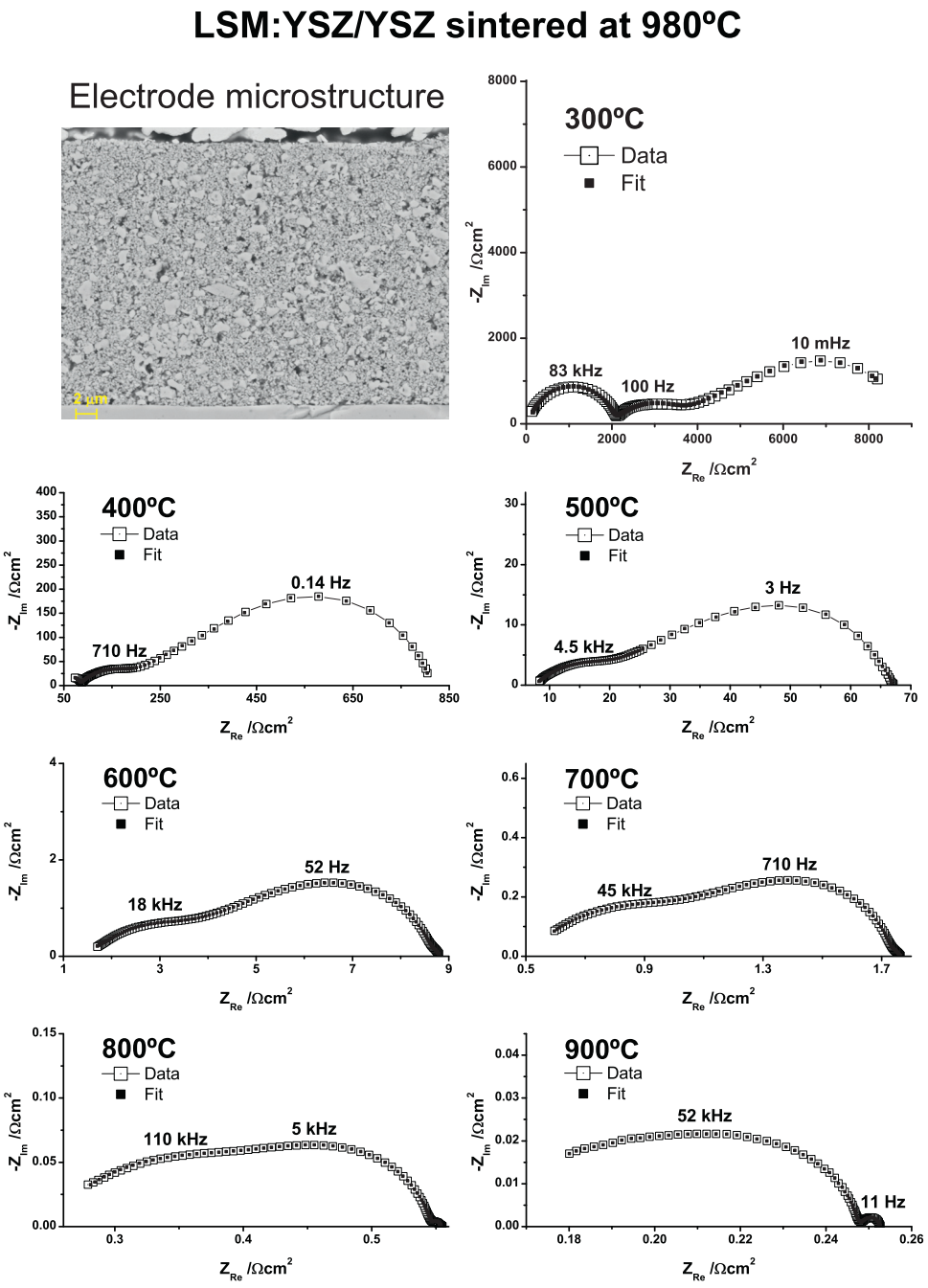

Fig. 6. Impedance spectra in the temperature range 300–900 °C of a LSM:YSZ composite cathode on a YSZ electrolyte sintered at 980 °C. The low temperature spectra has been fitted with the equivalent circuit $(RQ)_1$–$(RQ)_2$–PET, while the high temperature spectra has been fitted with the equivalent circuit $R_s(RQ)_2$–PET–FLW.

in Figs. 3 and 5–8 it is clear that the ratio between grain interior and grain boundary resistance is very different in the two cases studied here, with YSZ and CGO electrolytes, respectively. This is due to the difference in activation energy of the grain interior and grain boundary resistances for the YSZ and the CGO electrolytes. For YSZ the activation energy for the grain boundary resistance is only slightly higher than that for the grain interior resistance [31]. For CGO the activation energy for the grain boundary resistance is significantly larger than that for the grain interior resistance [33]. The GI resistance is therefore significantly smaller than the GB resistance at low temperatures for CGO. Thus, arc I plus arc II is the EIS response from the used polycrystalline electrolytes. The impedance of the LSM:CGO cathodes on a CGO electrolyte in Fig. 8 is particularly simple since the equivalent circuit $(RQ)_{GI}(RQ)_{GB}$PET can fully account for the impedance. Comparing the impedance of the 1180 °C sintered LSM:CGO/CGO, LSM:YSZ/CGO and LSM:YSZ/YSZ assemblies, the presence of an extra arc III is clear for the YSZ containing assemblies. A reduction in sintering temperature from 1180 °C to 1080 °C of LSM:YSZ/YSZ diminishes the extra arc III, but it is still present most evident when the fitting of the spectra is performed. However, when the sintering temperature of LSM:YSZ/YSZ is even further reduced from 1080 °C to 980 °C, the extra arc III seems to be completely absent as it both visually and fitting wise cannot be detected. This sintering temperature dependency of arc III and the correlation to the presence of LSM/YSZ interfaces in the studied cathodes, point towards the interpretation that arc III is associated with the formation of secondary phases at LSM/YSZ interfaces. As arc III is present in the spectra of the LSM:YSZ/CGO

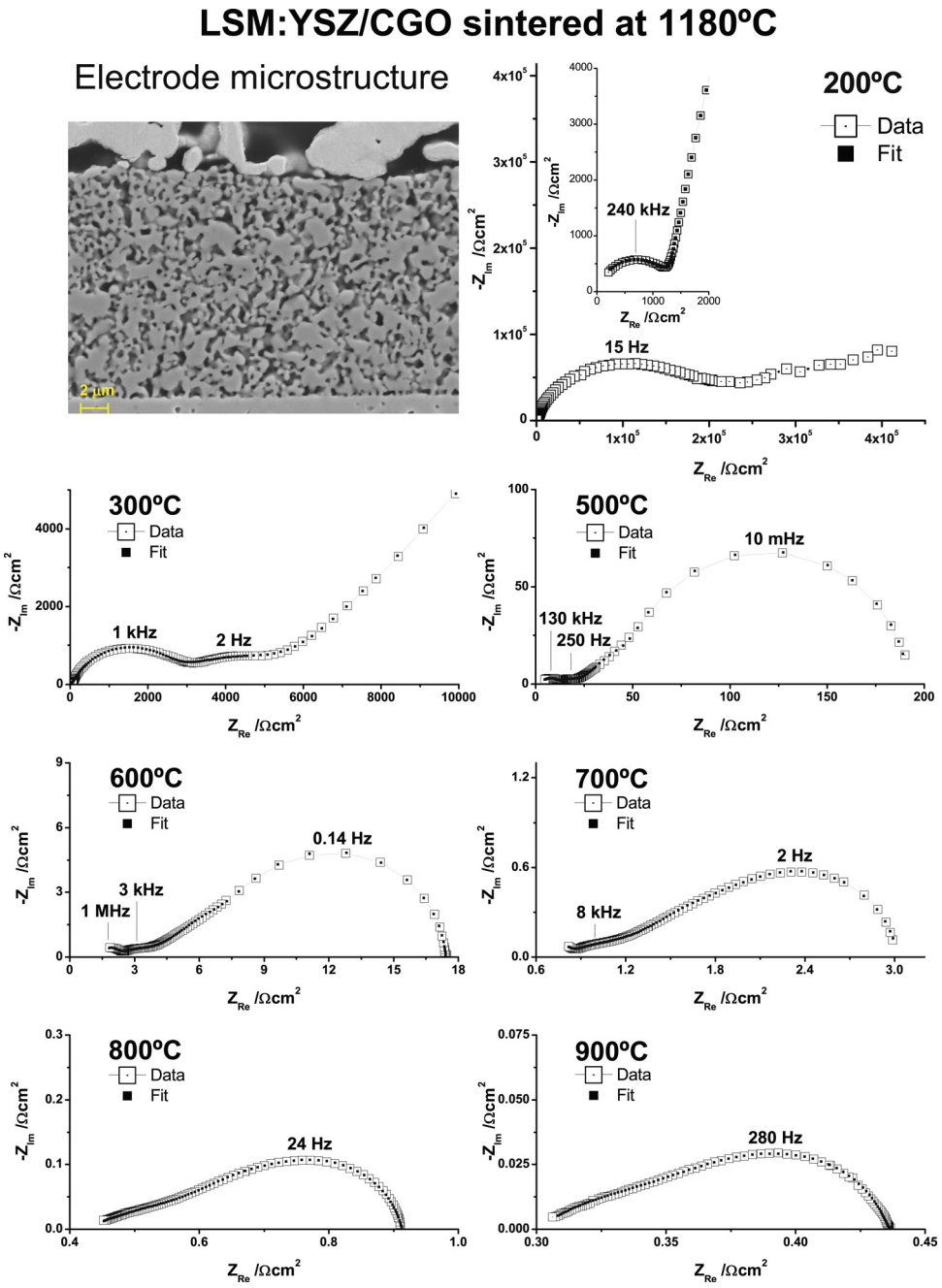

Fig. 7. Impedance spectra in the temperature range 200–900 °C of a LSM:YSZ composite cathode on a CGO electrolyte sintered at 1180 °C. The impedance spectra in the temperature range 300–700 °C has been fitted with the equivalent circuit $(RQ)_1$–$(RQ)_2$–PET, while the spectra above 700 °C has been fitted with the equivalent circuit $(RQ)_2$–PET.

assembly in Fig. 7 and not in the spectra of the LSM:CGO/CGO assembly in Fig. 8 it seems reasonable to conclude that the arc III is a consequence of secondary phases at the LSM/YSZ interfaces within the composite cathode of the LSM:YSZ/CGO assembly. This is discussed further in the following section concerned with the PET EIS model.

5.2. PET as EIS model

From the impedance data in Figs. 3 and 5–8 it is clear that the PET de Levie model is describing the data very well. For all the cathode/electrolyte combinations the characteristic skewed semicircle can be observed. As expected from the PET de Levie EIS model the variation in $P(O_2)$ in Fig. 4 can convincingly solely be accounted for by a change in the impedance of the surface reaction ζ. The cathodes sintered at the highest temperatures, and thus with a higher impedance of the surface reaction ζ, changes shape in excellent accordance with the predictions of the PET de Levie model as the temperature is lowered. The temperature dependence of the characteristic electrochemical utilization thickness λ depends on the activation energy of the involved PET de Levie parameters r_c and r_r. If $E_a(r_r) > E_a(r_c)$ then λ will increase with decreasing temperature, which is the case of the present study as can be seen in Fig. 9. A further support of the PET de Levie model is that the extracted activation energies of the involved PET de Levie parameters such as r_c and r_r are in excellent agreement with the reported materials

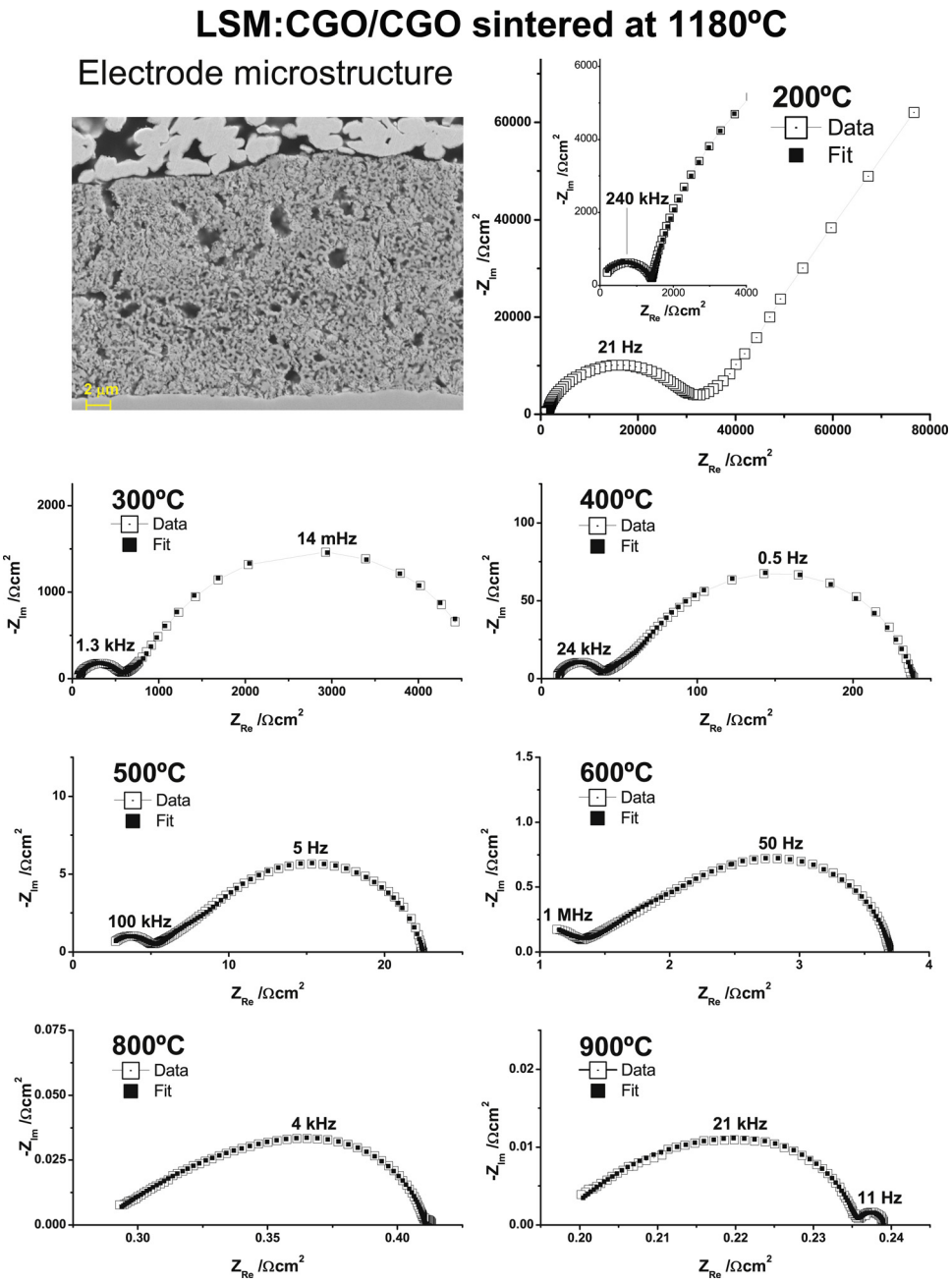

Fig. 8. Impedance spectra in the temperature range 200–900 °C of a LSM:CGO composite cathode on a CGO electrolyte sintered at 1180 °C. The impedance spectra from 300 °C to 750 °C has been fitted with the equivalent circuit $R_s(RQ)_2$–PET, while the spectra from 800 °C has been fitted with the equivalent circuit $R_s(RQ)_2$–PET–FLW.

parameters found in literature. This will be discussed in detail in Section 5.3. In the previous Section 5.1 arc III was identified as originating from the LSM/YSZ interfaces within the composite cathode. The implication of this is that the PET transmission line response describing the porous electrode, should somehow be modified to account for arc III. The LSM/YSZ impedance may deviate from the (RQ) arc assumed in Eq. (5) as published studies on LSM point electrodes also indicate. This is discussed further in the literature review in Section 6.2. From these LSM point electrodes studies an extra high frequency feature is usually observed. Whether a modification of the impedance in Eq. (5) of the PET impedance response can account for arc III in Figs. 3, 5 and 7 is difficult to say. Arc III and the grain boundary arc II show a strong overlap and thus the specific shape of arc III is difficult to resolve and hence fit. For a more complete elucidation on the impact of secondary phases at the LSM/YSZ interface on the shape of the high frequency PET impedance response, measurements should be performed on YSZ single crystals. In the present study we model the charge transfer across the formed layer of secondary phases at the LSM/YSZ TPB by a simple (RQ) arc for simplicity reasons. In the context of secondary phases at LSM/YSZ interfaces one may wonder whether there is a significant impedance contribution from LSM cathode particles in direct contact with the YSZ electrolyte, particles thus located at the cathode/electrolyte interface. This impedance $Z_{LSM/electrolyte}$ contribution has been neglected in the theoretical treatment in Section 2. The impedance $Z_{LSM/electrolyte}$ is in parallel with the PET transmission line. The impedance of the PET transmission line is in practise, with the used composite electrolyte materials, many

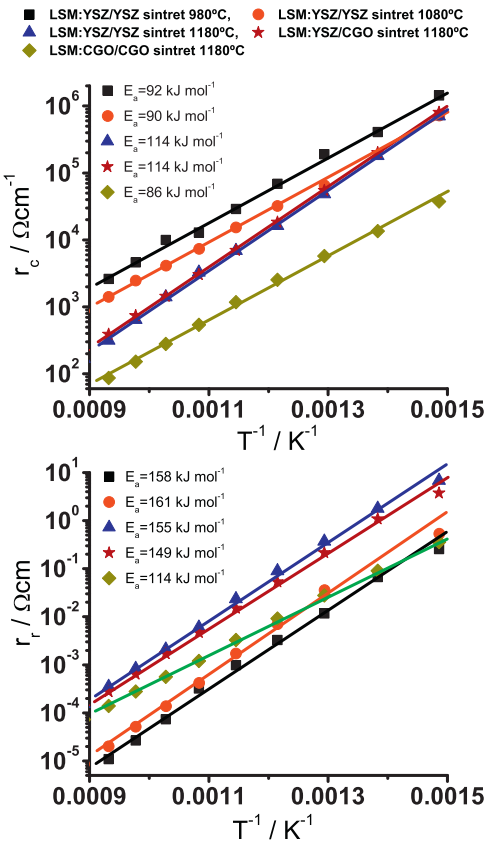

Fig. 9. Arrhenius plots of fitted porous electrode theory de Levie r_c and r_r parameters.

times smaller than $Z_{LSM/electrolyte}$ and is thus the impedance contribution which controls the overall impedance response. It is well known, that making the SOFC electrode a composite improves the electrode performance considerably, which is the reason why all non-MIEC-based SOFC electrodes today are composite electrodes. Thus, the assumptions in Section 2 are reasonable and EIS effects from secondary phases at the cathode/electrolyte interface are negligible. Furthermore, an impedance contribution in parallel with the PET de Levie impedance cannot give rise to an extra arc as arc III.

5.3. Overall discussion of results

Starting with the magnitude of the determined de Levie PET fit parameters r_c and r_r in Fig. 9 it can be seen that r_c decreases as the sintering temperature for the LSM:YSZ cathode is increased from 980 °C to 1180 °C. This is as expected since the necking between the individual YSZ grains within the cathodes gets better with increasing sintering and hence temperature. Similarly it is possible to see that r_r increases since the LSM/YSZ TPB length decreases as the cathode grains grow with increasing sintering temperature. Furthermore, it is also possible to see that both r_c and r_r are smaller for the LSM:CGO cathode compared to the LSM:YSZ cathode sintered at a similar temperature of 1180 °C.

Firstly the LSM:YSZ and the LSM:CGO cathode screen printing pastes are different leading to two different microstructures that are not directly comparable. Secondly the around 8 mol% Mn dissolved in YSZ when sintered at 1180 °C lowers the YSZ conductance [34]. Mn is not dissolved to nearly the same degree in CGO [2]. Manganese solubility and solubility kinetics is discussed in detail later in the section. An activation energy of 86 kJ/mol for r_c in the case of CGO is a realistic value, especially when considering the expected significant conductivity contribution from the grain boundaries in the percolated submicron sized cathode CGO grain network [33]. The pronounced lower activation energy of 114 kJ/mol for the LSM:CGO TPB represented by r_r compared to that of LSM:YSZ is an interesting finding. Recently H. Yokokawa has by combined ^{18}O isotope exchange and SIMS measurements shown that CGO has a catalytic effect on the oxygen reduction reaction (ORR) [35]. A lowering in the activation energy of the TPB reaction has also been observed when LSM:YSZ cathodes has been infiltrated with minor amounts of CGO [36]. This could potentially explain the lowering in the activation energy of the LSM:CGO TPB reaction. In Fig. 9 activation energies are determined from the fits of the different cathode/electrolyte combinations in Figs. 3 and 5–8 for the PET de Levie parameters r_c and r_r. The activation energies are for convenience summarized in Table 1. The observed $E_a(r_r)$ values for the LSM:YSZ cathodes are ranging from 149 kJ/mol to 161 kJ/mol. For the LSM:YSZ cathodes sintered at 980 °C and 1080 °C, similar $E_a(r_c)$ values of 90 kJ/mol and 92 kJ/mol are obtained. For the two LSM:YSZ cathode/electrolyte assemblies sintered at 1180 °C a somewhat higher value of 114 kJ/mol was obtained. Values for the activation energy of oxide ion conduction in the used YSZ can in literature be found to range from 85 kJ/mol to 97 kJ/mol [37–39]. This is in excellent agreement with the estimated 90 kJ/mol and 92 kJ/mol $E_a(r_c)$ values for the 980 °C and 1080 °C sintered LSM:YSZ cathodes. The Mn solubility in YSZ and the effect of dissolved Mn in YSZ has carefully been studied by Kawada et al. [34,40]. The solubility of Mn in YSZ was found to be 8 mol% at 1200 °C and 5 mol% at 1000 °C. The Mn solubility in YSZ at 1000 °C was determined by extrapolation from obtained Mn solubility data at higher temperatures. This was done since they were not able to detect any dissolved Mn in YSZ even after 50 h at 1000 °C, which they concluded was due to very slow Mn dissolution kinetics. These observations are in excellent agreement with the present results where the obtained $E_a(r_c)$ for the LSM:YSZ/YSZ samples sintered at 980 °C and 1080 °C closely corresponds to that of pure YSZ. Furthermore, Yokokawa and co-workers observed that the activation energy associated with the electrical conductivity increases with increasing amount of dissolved Mn in YSZ [34]. Their results are summarized in Table 2. Comparing the data in Table 2 with the acquired activation energy $E_a(r_c)$ of 114 kJ/mol for the 1180 °C sintered LSM:YSZ/YSZ and LSM:YSZ/CGO assemblies a good agreement with E_a of 10 mol% dissolved Mn in YSZ is seen. However, at 1180 °C it should only be possible to dissolve approximately 8 mol% Mn in YSZ according to their data. Nonetheless, the increase in $E_a(r_c)$ of the 1180 °C sintered cathodes convincingly indicates the dissolution of Mn in YSZ during sintering. With this in mind, it is noteworthy that the appearance of the additional arc III in the impedance spectrum coincides with the dissolution of Mn in YSZ. This indicates the formation of a resistive layer between LSM and YSZ, and agrees well with common understanding of the formation of secondary phases. The reactivity of various cathode materials and the YSZ electrolyte material has been studied to a large extent and is too large to cover in detail in the present paper. Instead the reader is referred to the already existing reviews on the subject for a comprehensive overview and detailed insight [2,23,24,26]. However, of particular interest in relation to the present results on LSM based cathodes is the paper by Mitterdorfer and Gaukler [24]. They studied zirconate formation ($La_2Sr_2ZrO_7$ and/or

Table 2
Correlation between dissolved Mn in YSZ and the activation energy for oxide ion conduction according to Ref. [34].

Dissolved Mn in YSZ (mol%)	2	6	10
Activation energy (kJ mol^{-1})	92	104	115

$SrZrO_3$) at the interface between LSM and YSZ with either excess or deficient Mn in the LSM structure. It was found that excess Mn can retard the formation of zirconate phases, while Mn deficient LSM readily forms zirconate phases at the LSM/YSZ interface. Thus, it appears appropriate that the additional arc III has been assigned to the formation of zirconates at the LSM/YSZ interface. This also explains why no additional arc III is seen for LSM:CGO/CGO, which also is sintered at 1180 °C. Taking the sluggish Mn dissolution kinetics into YSZ reported in [40] and the results of the present study into consideration one may think that there is no practical problem with Mn loss from LSM at the lower SOFC operating temperatures of 750–850 °C. However, there are other factors which affect the loss of Mn from LSM. Backhaus-Ricoult et al. has by TEM studies and in-situ studies of SOFC operating LSM:YSZ cathodes convincingly demonstrated that upon cathodic polarization Mn^{2+} spread to the LSM/YSZ interface and the three-phase-boundary (TPB) and from the TPB over to the YSZ electrolyte surface [41,42]. Furthermore, the presence of moisture in combination with polarization of the LSM:YSZ/YSZ cathode has been shown to lead to an increased degradation rate, which probably is due to an enhanced removal of Mn from the LSM/YSZ interface [43,44]. In these studies the moisture induced degradation was primarily caused by an increase of the LSM:YSZ/YSZ cathode high frequency arc with a summit frequency of around 25 kHz at 750 °C [44]. This corresponds well with the summit frequency of arc III in the present study. However, a similar effect of moisture was also seen on SOFC cells with a LSM:CGO/CGO cathode. Nonetheless, if Mn is removed from the LSM/YSZ interface the LSM perovskite structure will eventually decompose, and if YSZ is present zirconate phases will be formed. In the case of CGO a decomposed LSM layer would then, instead of zirconates be present at the LSM/CGO interface, which also will act as a barrier that can be seen as an extra arc in EIS. Thus, arc III could possibly be interpreted as a consequence of the loss of Mn from the LSM structure at the TPB reaction zone. The difference in the impedance of the LSM:YSZ/YSZ, the LSM:YSZ/CGO and the LSM:CGO/CGO 1180 °C sintered assemblies in Figs. 3 and 7–8 are therefore the difference in Mn dissolution/solubility in YSZ and CGO during sintering, respectively. It corresponds well with the understanding that LSM has a very good chemical stability with CGO [2].

From the fits with the PET de Levie EIS model it is possible to calculate the DC resistance R_p as a function of thickness L. This is for illustrative purposes done for the LSM:CGO/CGO assembly at 650 °C in the top of Fig. 10. From the figure it is also possible to see the characteristic electrochemical utilization thickness λ. At the bottom of Fig. 10 the utilization thickness λ is shown as a function of temperature. Thus, the use of PET de Levie EIS model can provide valuable engineering characteristics, which is difficult to acquire otherwise.

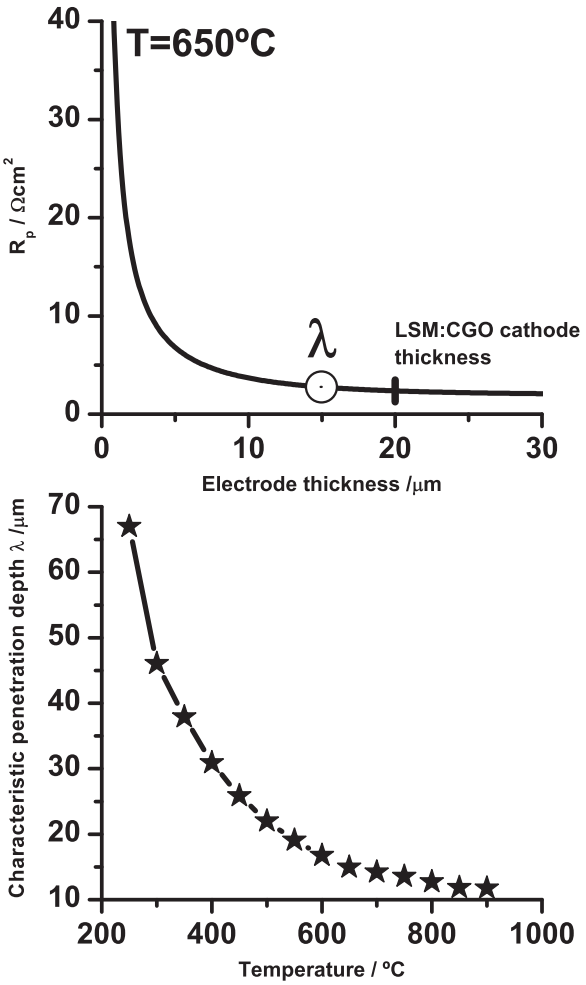

Fig. 10. Based on the porous electrode theory de Levie impedance model fits in Fig. 8 the following calculations have been made. At the top, the PET impedance model polarization resistance R_p as a function of electrode thickness L. At the bottom, the characteristic electrochemical utilization thickness λ as a function of temperature.

6. Literature survey

6.1. Mixed electronic ionic conducting cathodes

Consensus within the literature exists on that MIEC SOFC cathodes can appropriately be described by the Gerischer impedance, describing the co-limiting situation of coupled bulk oxide ion diffusion and surface reaction. This was in particular established by Adler et al. in their work on Electrode Kinetics of Porous Mixed-Conducting Oxygen Electrodes (ALS model) [45]. The derived ALS model is similar to the semi-infinite Gerischer impedance. However, in their work the Gerischer parameters were formulated in terms of bulk and surface material properties along with microstructural characteristics of the prepared cathodes. The EIS model was convincingly evaluated on $La_{0.6}Ca_{0.4}Fe_{0.8}Co_{0.2}O_{3-\delta}$ and $La_{1-x}Sr_xCo_{3-\delta}$ cathodes, where the extracted properties from the model were in well accordance with known literature values [45,46]. In the latter mentioned reference Adler et al. extended the ALS model by deriving the solution for the finite electrode thickness. The derived solution involves a hyperbolic cotangent (coth). This is in accordance with Eq. (3) and the Finite-Length-Gerischer expression derived by the author et al. of the present study in [29], where the composite electrode situation with a MIEC material in combination with an ionic conductor such as e.g. CGO is also discussed. However, this is unlike the Finite-Length-Gerischer expression derived by Boukamp and Bouwmeester, which involves a hyperbolic tangent (tanh) [47]. All the mentioned models describe the transmission to the left in Fig. 1 and they can therefore not all be correct. The correct expressions for the transmission line are the ones involving a hyperbolic cotangent (coth). The difference in the expressions lies in the use of a single boundary condition, when solving the associated differential equation for the situation. This is carefully discussed in details in [29]. Further support for an expression involving coth, besides the vast literature on porous electrode theory applied to electrochemistry at solid/liquid interfaces comes from electrochemical performance modelling of MIEC cathodes. Polarization mechanisms and modelling of the electrochemical performance have been reviewed by Fleig in [48]. In here, the literature on continuum electrode modelling was reviewed

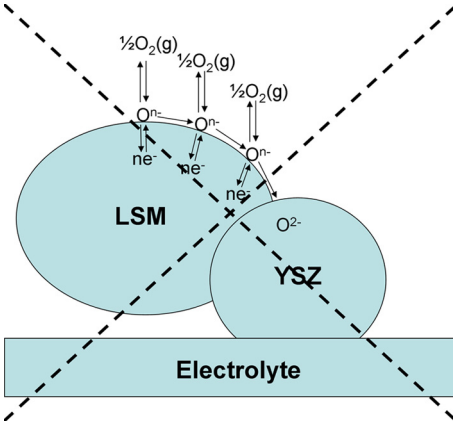

Fig. 11. An often proposed reaction mechanism in the literature to explain an observed skewed semicircle impedance shape. However, this is a false interpretation as discussed in the text.

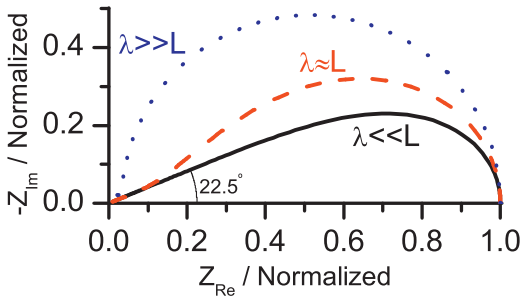

Fig. 12. The implication of a semi-infinite Gerischer type impedance response depicted in Fig. 11 as the electrochemical surface impedance ζ in Eq. (5) of the porous electrode theory. The EIS response has a characteristic 22.5 degree high frequency slope. This has never been observed for SOFC electrodes. Thus, the Gerischer type mechanism in Fig. 11. can be excluded.

and the following expression was derived, which essentially is the direct current (DC) case of Eq. (3):

$$\tilde{R} = \sqrt{\frac{1}{\bar{\sigma}_{\text{ion}} Y_{\text{vol}}}} \coth\left(L\sqrt{\frac{Y_{\text{vol}}}{\bar{\sigma}_{\text{ion}}}}\right) \tag{8}$$

where $\tilde{R}$ is the area specific polarization resistance, $\bar{\sigma}_{\text{ion}}$ is an effective ionic conductivity, Y_{vol} is a volumetric source rate constant describing the "readiness" of the cathodic reaction and L is the cathode thickness.

The impedance model derived by Adler et al. is the ideal case with no suppression of the response. It corresponds to modelling the reaction in Eq. (5) as a resistor in parallel with a capacitor. However, ideal capacitances are rarely observed in electrochemistry. Instead a much more applicable approach is the use of a CPE. Using a CPE in Eq. (5) and hence in the transmission line of Fig. 1 provides a suppression of the impedance response.

6.2. Composite cathodes

Since the work of Adler et al. on Electrode Kinetics of Porous Mixed-Conducting Oxygen Electrodes presented in Section 6.1, and the Adler review on SOFC cathodes in 2004 [26], there has been a tendency in the SOFC community to refer to a skewed semicircle as a Gerischer impedance describing the coupling between diffusion and reaction. However, the coupling between the oxide ionic conduction in the ionically conducting network of a composite cathode with the electrochemical reaction at e.g. the TPB also results in a skewed semicircle as accounted for in the theory (Section 2). Thus, it seems that SOFC researchers when they have encountered something that looks like a skewed semicircle associated this with a Gerischer impedance. However, a Gerischer impedance implies that oxide ions are diffusing, which is obvious for MIEC materials but not for a pure electronic conducting material such as LSM. This has lead some researchers to conclude that a Gerischer like impedance is due to a coupling between oxygen surface diffusion and oxygen adsorption on LSM as illustrated in Fig. 11 [24,26,49–54]. Adler has in his extensive review on SOFC cathodes in 2004 [26] argued that such a coupling between surface diffusion and oxygen adsorption can be seen in EIS. However, direct experimental evidence is sparse despite the huge research efforts in understanding the oxygen reduction reaction (ORR) on Pt etc and in SOFC cathodes during the last 50–100 years. It is a very intuitive and appealing reaction mechanism and Mitterdorfer and Gauckler has e.g. argued that the Gerischer impedance is not seen because it is overshadowed by the double layer capacitance C_{dl}. Therefore by subtracting the C_{dl} they claim that a Gerischer impedance can be resolved as they have illustrated for LSM and Pt in [24,54]. However, manipulation of the EIS data is a delicate procedure. The magnitude of C_{dl} is in principle not known neither is the degree of semicircle suppression or in other words the CPE behaviour of the double layer capacitance C_{dl}. Thus, if they are correct a Gerischer impedance can in principle be resolved directly if a sufficiently favourable ratio between the TPB length and cathode/electrolyte area is obtained. However, no such reports exist to the best of our knowledge.

From the present study it is clear that the composite structure with electronically and ionically conducting networks in itself results in a skewed semicircle according to the PET de Levie theory in Section 2. If it is true that the LSM/YSZ TPB reaction is a Gerischer with a coupling between surface diffusion and adsorption according to Fig. 11, then a Gerischer impedance should replace the suppressed semicircle in Eq. (5) modelling ζ in the transmission PET de Levie model. If a semi-infinite Gerischer response is put into Eq. (5), the result would be the responses depicted in Fig. 12. The implication is a characteristic 22.5° high frequency slope. However, this has never been reported for SOFC electrodes, which furthermore is in disfavour of the Gerischer mechanism of Fig. 11. Another argumentation that the mechanism in Fig. 11 cannot account for the present results is the following: The Finite response is seen of the high temperature well sintered cathodes with large particles, while the semi-infinite response is seen for the low temperature sintered cathodes with small particles. With the extracted activation energies in Fig. 9 it should be the other way around according to the mechanism in Fig. 11. Thus, again the mechanism in Fig. 11 cannot be true. At present there is simply not sufficient solid experimental evidence for a mechanism such as that in Fig. 11.

Point electrode measurements have usually reported a suppressed semicircle response, but sometimes with a small and poorly resolved high frequency feature due to secondary phases at the LSM/YSZ interface [1,55–57]. Jørgensen noted in her review on LSM:YSZ composite cathodes from 2001 [1] that LSM:YSZ composite cathodes are much more complicated than LSM pointed cathodes, which in fact is due to the coupled impedance of the PET de Levie model. They were able to detect up to five RQ arcs by varying parameters such as the cathode sintering temperature, measuring temperature and oxygen partial pressure. However, the main ('electrochemical') impedance response could be described by two suppressed semicircles. Similar conclusions have been reported in the review on LSM cathodes by Jiang in 2008 [2]. This is also what typically is used for the evaluation of infiltrated LSM:YSZ composite cathodes [36,58] or in the breakdown of losses in anode supported SOFCs with LSM:YSZ cathodes [44,59]. SOFCs with LSM based cathodes were at least originally thought to be operated at high temperatures of 800–1000 °C. Looking for example at the EIS spectra in temperature range 800–900 °C of the 980 °C and 1080 °C

sintered cathodes in Figs. 5–6, where the impedance contributions strongly overlap, it is clear why people have described the LSM:YSZ impedance by two semicircles. However, upon a lowering of the temperature it becomes quite clear that two suppressed semicircles cannot account for the impedance. Bonanos et al. measured, for the first time, a composition-wise graded LSM:YSZ composite cathode impedance over a very broad and relative low temperature range from 700 °C to 300 °C [60]. The results were completely resolved impedance spectra, which also exhibited the transition from a skewed semicircle to a semicircle as in Figs. 3, 7 and 8. The impedance was analyzed in terms of a sufficient number of (RQ) arcs and later on, the spectra were also analyzed in terms of a semi-infinite Gerischer impedance response in [61]. The impedance shapes and shape change were partly explained as a consequence of the smearing out effects of the graded structure. However, the observations are as in the present study a consequence of the PET de Levie EIS model. As for MIEC cathodes in Section 6.1 continuum modelling considerations for LSM:YSZ composite cathodes has also lead to an expression for the polarization resistance, which involve a hyperbolic cotangent (coth) dependency as a function of electrode thickness in accordance with the DC limiting case of the PET de Levie model Eq. (3) [48,62,63].

6.3. Composite anodes

A review on anode materials has been given in 2004 by Jiang and Chan [3]. In the context of EIS of composite anodes we will in the following limit the discussion for brevity to the classic Ni:YSZ composite SOFC anode. Brown et al. have through the matrix of experiments in Ref. [64] illustrated the situation more or less. For pure Ni electrodes on YSZ the electrochemistry can be very well described by a suppressed semicircle as illustrated by Ni paste and Ni felt model anodes. However, upon putting Ni into a YSZ network and thereby forming a Ni:YSZ composite electrode a change in the impedance shape is clearly seen from a semicircle to that of a skewed semicircle. The observations are analogous to those Jørgensen reported in her review on LSM cathodes [1] and which was discussed in the previous Section 6.2. The skewed semicircle impedance response of Ni:YSZ has as for LSM:YSZ composite cathodes incorrectly been interpreted as a Gerischer response and thereby as a mechanism similar to that of Fig. 11 with a coupling between surface diffusion and an adsorption reaction [51–53,65]. However, as mentioned in the introduction Sonn et al. has performed an analysis of the Ni:YSZ anode with the PET de Levie EIS model in [21]. Despite that they did not show any of the performed fits the extracted parameters from the PET de Levie model were in excellent accordance with known literature values. Furthermore, they also illustrated how two (RQ) arcs is a good approximation to the skewed semicircle impedance shape of the PET de Levie model. As a rough approximation one could say that the high frequency (RQ) arc is the ionic conduction in the composite electrode, while the low frequency (RQ) arc is the surface/TPB reaction.

6.4. Composite electrodes prepared by infiltration

For a number of reasons there is an increasing interest in composite SOFC electrodes prepared by coating a thin layer of material on a scaffold/backbone by infiltration. Jiang has reviewed the advances in the area in a number of papers [36,58]. The scaffold is typically either a pure ionic conductor or electronic conductor. The scaffold is then coated by a thin layer via infiltration with a material so that an electrode with both an ionically and an electronically conducting network is obtained. Thus, as for composite SOFC cathodes and anodes the PET de Levie EIS model is applicable. An anode for MS-SOFC consisting of a FeCr scaffold infiltrated with small amounts of Ni in CGO has for instance successfully been analyzed in terms of the PET de Levie EIS model in [22]. However, the impedance of infiltrated electrodes has so far usually been analyzed in terms of (RQ) arcs as other SOFC composite electrodes. Electrodes infiltrated with Pd have been studied extensively according to Jiangs review [58]. However, Pd has been shown to result in current fluctuations and Pd migration upon polarization [66]. This is most likely the cause to the peculiar impedance spectra of the Pd infiltrated electrodes shown in [58]. For such non-stationary electrodes the PET de Levie EIS model is for obvious reasons not valid.

7. Dispersion effects

The continuum porous electrode theory modelling presented in Section 2 essentially assumes that the whole electrode is one phase with certain non-distributed properties. It corresponds to looking at the electrode from a far distance without realizing any inhomogeneities such as different phases, microstructural inhomogeneities or spatial inhomogeneous electrochemical activities—e.g. TPB phenomena [48]. Instead a homogenous effective electrode phase with effective properties is assumed. Thus, in this approach there is no difference between MIEC electrodes or composite electrodes and they can therefore be described by the same transmission line as illustrated in Fig. 1. This is of course a simplification of the real situation. Nonetheless, the averaging with effective values does seem to work very well in practise. This is for example illustrated by the results presented in Section 4, where very good fits were obtained and physical properties in accordance with literature values were extracted. Imperfections such as large pores, cracks, single-phase agglomerates, etc in the microstructure have the effect that L representing the electrode thickness in Eqs. (1) and (3) is not single valued but distributed. It corresponds to a distribution in the column height in Fig. 1. The effect has been studied in [29,67,68]. In here, it is shown how the transition from a 45° HF slope to a semicircle for the $L \sim \lambda$ case in Fig. 2 becomes smoother as L becomes more distributed. Columns with a small height contribute with a semicircle response, while tall columns contribute with a skewed semicircle. The overall EIS response depends on the distribution in column height. Kreller and Adler have studied the effect of a surface pathway in parallel with the typical Gerischer response with bulk oxide ion vacancy diffusion. They found that the addition of a surface pathway can result in a more elongated Gerischer type EIS response [69]. In Fig. 1 the microstructure is modelled as columns in analogy with porous electrode theory where the pore of solid porous electrodes in liquid electrolytes is modelled as cylinders. Deviations from cylindrical pores have been studied in [70–72], where it is shown how such effects also may distort the porous electrode theory EIS shape. Thus, there are a number of effects which may give rise to distributed properties and greater frequency dispersion compared to the EIS response predicted by porous electrode theory. A way to describe such dispersions in the fitting of impedance data is to use a fractal approach as proposed by Boukamp et al. in [47], where furthermore the exponent of the square root 0.5 is adjustable. However, it increases the number of free variables and the possible impedance shapes considerably and is associated with an interpretation, which is somewhat looser than the use of a CPE in the de Levie transmission line. The assumptions in Eqs. (4) and (5) also need to be fulfilled in order for the PET de Levie EIS response to be valid. However, it is striking how often that the electrochemical reaction presented in Eq. (5) can be described by a suppressed semicircle, but deviations may in principle occur. Nonetheless, this can of cause be checked by measurements on point electrodes. Even if the electrochemical impedance response deviate from a (RQ) suppressed semicircle, PET is still valid, but the situation may become significantly more complicated.

Table 3
Physical interpretation of the transmission line impedance parameters for the Gerischer and the PET de Levie impedance response.

Impedance element	Gerischer	Porous electrode theory de Levie
r_c	Resistance associated with oxygen vacancy diffusion in the MIEC phase	Electrolyte resistance
r_r	MIEC/gas phase interfacial chemical reaction resistance	Electrode reaction resistance at e.g. the TPB
Q	Chemical capacitance associated with changes in MIEC oxygen stoichiometry	Electrode/electrolyte interfacial double layer capacitance

8. Overall discussion

From the results on LSM based composite cathodes and the literature review/discussion on other types of SOFC electrodes, it is clear that the transmission line description is the correct interpretation and model for SOFC electrodes. It is the correct interpretation for any type of electrode, which consist of interpenetrating ionically and electronically connected networks. From the results and the literature review it is also clear that the Gerischer interpretation made by many researchers and associated with a coupling between surface diffusion and adsorption is incorrect. Instead one should use PET when the characteristic skewed semicircle is encountered for SOFC composite electrodes. The term Gerischer impedance is strictly speaking only valid for SOFC MIEC cathodes where bulk oxide ion vacancy diffusion takes place. In the Gerischer case with diffusion, the ionic transport is driven by a gradient in the chemical potential, while in porous electrode theory case with ionic conduction, the ionic transport is driven by a gradient in the electrical potential. They share the same transmission line in Fig. 1, but the interpretations of the involved parameters are different. An overview of the parameter interpretation in the two cases is given in Table 3.

A simplified impedance evaluation in the form of a sufficient number of serially connected (RQ) suppressed semicircles is of course in many cases an acceptable starting point and a suitable approximation. The interpretation of the (RQ) arcs to a specific process usually requires an extensive test matrix. Furthermore, in some cases it is also not correct to ascribe an (RQ) arc to a specific process, since processes can be coupled as mentioned in the introduction. The term goodness of fit has sometimes been used to justify the use of a specific equivalent circuit. The use of serially connected (RQ) elements usually provides good fits. This is in many cases a false reassurance since a sufficient number of (RQ) arcs, (RQ) arc overlap, and different degrees of (RQ) suppression practically always can result in a nice fit. Such an approach also hides away dispersion effects in the electrodes. Instead EIS equivalent circuits and models should be evaluated based on whether they make physical sense, can account for variation in experimental parameters and the power to predict responses. A way to take the dispersion effects in Section 7 into consideration is to make Eqs. (1) and (3) fractal in a similar fashion to that in [47], which also briefly was mentioned in Section 7. However, this may give better fits but as a result the extracted physical parameters will have odd units, which e.g. make comparison among electrodes confusing and difficult. Finally, the characteristic skewed semicircle shape is for well performing electrodes distorted by the inductance from wires etc. and the high frequency region is poorly resolved due the practical frequency range limitations imposed on the EIS measurement. This illustrates the need to study the electrodes in a very broad temperature and parameter range in order to acquire an in-depth understanding of the electrodes. Under any circumstance it is clear from the present comprehensive cathode LSM:YSZ EIS study and literature review, that the transmission line description should form the basis for any SOFC electrode evaluation.

9. Conclusions

The comprehensive impedance study of technological relevant LSM based composite cathodes over a very broad temperature range with variation in sintering temperature, and thus microstructure, along with changes in the composite and electrolyte material from YSZ to CGO illustrate the various possible impedance features for LSM based composite cathodes. From these studies it is also clear that porous electrode theory is applicable to and a suitable framework for analysis of LSM based composite cathodes and in general porous composite SOFC electrodes. From the impedance CNLS fitting, activation energies in excellent accordance with known literature values were obtained. For example, an increase in the activation energy of YSZ composite material could be detected as the sintering temperature was increased, which indicates that Mn is dissolved in YSZ. Furthermore, as Mn is dissolved in the YSZ composite material the appearance of an extra arc at high frequencies could be detected, indicating the formation of resistive secondary phases at the LSM/YSZ interface. The analysis with PET could also provide desirable information from an engineering perspective, such as the electrochemical utilization thickness. Lastly, it was possible from the impedance study and the subsequent analysis using PET to rule out the Gerischer mechanism with a coupling between surface diffusion and adsorption on LSM which has been assumed by several SOFC researchers.

The present study clearly shows that the framework for any analysis of porous SOFC electrodes should have its origin in the transmission line model description. If the electrode ionic transport is governed by ionic conduction the framework of porous electrode theory is appropriate, whereas if the ionic transport is by diffusion the framework of the Gerischer impedance or equivalently the ALS model is appropriate.

Acknowledgements

The authors gratefully acknowledge financial support from Energinet.dk through the ForskEL programme under the projects Durable and Robust SOFC (2010-1-10441) and Towards Smart Grid Ready SOFC (2012-1-10747).

References

[1] M.J. Jørgensen, M. Mogensen, Impedance of Solid Oxide Fuel Cell LSM/YSZ Composite Cathodes, J. Electrochem. Soc. 148 (2001) A433.
[2] S.P. Jiang, Development of lanthanum strontium manganite perovskite cathode materials of solid oxide fuel cells: a review, J. Mater. Sci. 43 (2008) 6799.
[3] S.P. Jiang, S.H. Chan, A review of anode materials development in solid oxide fuel cells, J. Mater. Sci. 39 (2004) 4405.
[4] I.D. Raistrick, D.R. Franceschetti, J. Ross Macdonald, in: E. Barsoukov, J. Ross Macdonald (Eds.), Impedance Spectroscopy: Theory, Experiment and Applications, second ed., John Wiley & Sons, 2005, p. 57.
[5] T. Jacobsen, P.V. Hendriksen, S. Koch, Diffusion and conversion impedance in solid oxide fuel cells, Electrochim. Acta 53 (2008) 7500.
[6] H. Gerischer, Wechselstrompolarisation von Elektroden mit einem potentialbestimmenden Schritt beim Gleichgewichtpotential I, Z. Phys. Chem. 198 (1951) 286.
[7] R. de Levie, Electrochemical Responses of Porous and Rough Electrodes, in: P. Delahay (Ed.), Advances in Electrochemistry and Electrochemical Engineering, 6, Interscience, New York, 1967, p. 329.
[8] A. Lasia, Modeling of impedance of porous electrodes, in: M. Schlesinger (Ed.), Modern Aspects of Electrochemistry, 43, Springer, 2009, p. 2029.
[9] B.E. Conway, Electrochemical Supercapacitors, Kluwer Academic/Plenum Publishers, New York, 1999, pp. 377.
[10] R. Kötz, M. Carlen, Principles and applications of electrochemical capacitors, Electrochim. Acta 45 (2000) 2483.
[11] E. Barsoukov, J.H. Kim, J.H. Kim, C.O. Yoon, H. Lee, Kinetics of lithium intercalation into carbon anodes: in situ impedance investigation of thickness and potential dependence, Solid State Ionics 116 (1999) 249.

[12] A. Lundqvist, G. Lindbergh, Kinetic study of a porous metal hydride electrode, Electrochim. Acta 44 (1999) 2523.
[13] M. Maja, C. Orecchia, M. Strano, P. Tosco, M. Vanni, Effect of structure of the electrical performance of gas diffusion electrodes for metal air batteries, Electrochim. Acta 46 (2000) 423.
[14] W.J. Albery, A.R. Mount, Transmission Lines for Conducting Polymers, in: M.E.G. Lyons (Ed.), Electroactive Polymer Electrochemistry, Plenum Press, New York, 1944, p. 443.
[15] J. Bisquert, G.G. Belmonte, F.F. Santiago, N.S. Ferriols, M. Yamashita, E.C. Pereira, Application of a distributed impedance model in the analysis of conducting polymer films, Electrochem. Commun. 2 (2000) 601.
[16] J. Bisquert, G. Garcia-Belmonte, F. Fabregat-Santiago, A. Compte, Anomalous transport effects in the impedance of porous film electrodes, Electrochem. Commun. 1 (1999) 429.
[17] J. Bisquert, G. Garcia-Belmonte, F. Fabregat-Santiago, N.S. Ferriols, P. Bogdanoff, E.C. Pereira, Doubling Exponent Models for the Analysis of Porous Film Electrodes by Impedance. Relaxation of TiO_2 Nanoporous in Aqueous Solution, J. Phys. Chem. B 104 (2000) 2287.
[18] M.C. Lefebvre, R.B. Martin, P.G. Pickup, Characterization of Ionic Conductivity Profiles within Proton Exchange Membrane Fuel Cell Gas Diffusion Electrodes by Impedance Spectroscopy, Electrochem. Solid-State Lett. (1999) 259.
[19] N. Wagner, Electrochemical Impedance Spectroscopy, in: H. Wang, X. Yuan, H. Li (Eds.), PEM Fuel Cell Diagnostic Tools, CRC Press, Boca Raton, FL, 2012, p. 37.
[20] A. Hahn, H. Landes, Investigations into the Kinetics of SOFC Cathodes, in: U. Stimming, S.C. Singhal, H. Tagawa, W. Lehnert (Eds.), Paper Presented at SOFC V Electrochemical Proceedings, vol. 97, The Electrochemical Society, Pennington, NJ, 1997, p. 595.
[21] V. Sonn, A. Leonide, E. Ivers-Tiffeé, Combined Deconvolution and CNLS Fitting Approach Applied on the Impedance Response of Technical Ni/8YSZ Cermet Electrodes, J. Electrochem. Soc. 155 (2008) B675.
[22] J. Nielsen, T. Klemensø, P. Blennow, Detailed impedance characterization of a well performing and durable Ni:CGO infiltrated cermet anode for metal-supported solid oxide fuel cells, J. Power Sources 219 (2012) 305.
[23] T. Kawada, N. Sakai, H. Yokokawa, M. Dokiya, I. Anzai, Reaction between solid oxide fuel cell materials, Solid State Ionics 50 (1992) 189.
[24] A. Mitterdorfer, L.J. Gauckler, $La_2Zr_2O_7$ formation and oxygen reduction kinetics of the $La_{0.85}Sr_{0.15}Mn_yO_3$, $O_2(g)$|YSZ system, Solid State Ionics 111 (1998) 185.
[25] F.W. Poulsen, N. van der Puil, Phase relations and conductivity of Sr- and La-zirconates, Solid State Ionics 53–56 (1992) 777.
[26] S.B. Adler, Factors governing oxygen reduction in solid oxide fuel cell cathodes, Chem. Rev. 104 (2004) 4791.
[27] T. Jacobsen, B. Zachau-Christensen, L. Bay, S. Skaarup, SOFC Cathode Mechanisms, in: Proceedings of the 17th Risø International Symposium on Materials Science: High Temperature Electrochemistry: Ceramics and Metals, 1996, p. 29.
[28] B.A. Boukamp, A nonlinear least squares fit procedure for analysis of immittance data of electrochemical systems, Solid State Ionics 20 (1986) 31.
[29] J. Nielsen, T. Jacobsen, M. Wandel, Impedance of porous IT-SOFC LSCF:CGO composite cathodes, Electrochim. Acta 56 (2011) 7963.
[30] F.E.G. Henn, R.M. Buchanan, N. Jiang, D.A. Stevenson, Permittivity and AC conductivity in yttria-stabilized zirconia, Appl. Phys. A 60 (1995) 515.
[31] M.J. Verkerk, B.J. Middelhuis, A.J. Burggraaf, Effect of grain boundaries on the conductivity of high-purity ZrO_2-Y_2O_3 ceramics, Solid State Ionics 6 (1982) 159.
[32] G.M. Christie, F.P.F. van Berkel, Microstructure - ionic conductivity relationships in ceria-gadolinia electrolytes, Solid State Ionics 83 (1996) 17.
[33] B.C.H. Steele, Appraisal of $Ce_{1-y}Gd_yO_{2-y/2}$ electrolytes for IT-SOFC operation at 500°C, Solid State Ionics 129 (2000) 95.
[34] T. Kawada, N. Sakai, H. Yokokawa, M. Dokiya, Reaction between solid oxide fuel cell materials, Solid State Ionics 50 (1992) 189.
[35] H. Yokokawa, Thermodynamic and SIMS analyses on the role of proton/water in oxygen reduction process and related degradations in solid oxide fuel cells, Solid State Ionics 225 (2012) 6.
[36] S.P. Jiang, A review of wet impregnation—An alternative method for the fabrication of high performance and nano-structured electrodes of solid oxide fuel cells, Mater. Sci. Eng., A 418 (2006) 199.
[37] M. Ghatee, M.H. Shariat, J.T.S. Irvine, Investigation of electrical and mechanical properties of 3YSZ/8YSZ composite electrolytes, Solid State Ionics 180 (2009) 57.
[38] P. Ried, C. Lorenz, A. Brönstrup, T. Graule, N.H. Menzler, W. Sitte, P. Holtappels, Processing of YSZ screen printing pastes and the characterization of the electrolyte layers for anode supported SOFC, J. Eur. Ceram. Soc. 28 (2008) 1801.
[39] O. Yamamoto, Y. Takeda, R. Kanno, K. Kohno, T. Kamiharai, Electrical conductivity of polycrystalline tetragonal zirconia ZrO_2-M_2O_3 (M = Sc, Y, Yb), J. Mater. Sci. Lett. 8 (1989) 198.
[40] T. Kawada, N. Sakai, H. Yokokawa, M. Dokiya, Electrical properties of transition-metal-doped YSZ, Solid State Ionics 53 (1992) 418.
[41] M. Backhaus-Ricoult, Interface chemistry in LSM–YSZ composite SOFC cathodes, Solid State Ionics 177 (2006) 2195.
[42] M. Backhaus-Ricoult, K. Adib, T. St Clair, B. Luerssen, L. Gregoratti, A. Barinov, In-situ study of operating SOFC LSM/YSZ cathodes under polarization by photoelectron microscopy, Solid State Ionics 179 (2008) 891.
[43] J. Nielsen, A. Hagen, Y.L. Liu, Effect of cathode gas humidification on performance and durability of Solid Oxide Fuel Cells, Solid State Ionics 181 (2010) 517.
[44] J. Nielsen, M. Mogensen, SOFC LSM:YSZ cathode degradation induced by moisture: An impedance spectroscopy study, Solid State Ionics 189 (2011) 74.
[45] S.B. Adler, J.A. Lane, B.C. Steele, Electrode Kinetics of Porous Mixed-Conducting Oxygen Electrodes, J. Electrochem. Soc. 143 (1996) 3554.
[46] S.B. Adler, Mechanism and kinetics of oxygen reduction on porous $La_{1-x}SrxCoO_{3-\delta}$, Solid State Ionics 111 (1998) 125.
[47] B.A. Boukamp, H.J.M. Bouwmeester, Interpretation of the Gerischer impedance in solid state ionics, Solid State Ionics 157 (2003) 29.
[48] J. Fleig, Solid oxide fuel cell cathodes: Polarization Mechanisms and Modeling of the Electrochemical Performance, Annu. Rev. Mater. Res. 33 (2003) 361.
[49] E.C. Shin, P.A. Ahn, H.H. Seo, J.M. Jo, S.D. Kim, S.K. Woo, J.H. Yu, J. Mizusaki, J.S. Lee, Polarization mechanism of high temperature electrolysis in a Ni–YSZ/YSZ/LSM solid oxide cell by parametric impedance analysis, Solid State Ionics 232 (2013) 80.
[50] P. Hjalmarsson, M. Mogensen, $La_{0.99}Co_{0.4}Ni_{0.6}O_{3-\delta}$–$Ce_{0.8}Gd_{0.2}O_{1.95}$ as composite cathode for solid oxide fuel cells, J. Power Sources 196 (2011) 7237.
[51] B.A. Boukamp, M. Verbraeken, D.H.A. Blank, P. Holtappels, SOFC-anodes, proof for a finite-length type Gerischer impedance? Solid State Ionics 177 (2006) 2539.
[52] P. Holtappels, J. Bradley, J.T.S. Irvine, A. Kaiser, M. Mogensen, Electrochemical Characterization of Ceramic SOFC Anodes, J. Electrochem. Soc. 148 (2001) A923.
[53] P. Holtappels, M. Verbraeken, U. Vogt, D.H.A. Blank, B.A. Boukamp, Preparation and electrochemical characterisation of supporting SOFC–Ni–YZT anodes, Solid State Ionics 177 (2006) 2029.
[54] A. Mitterdorfer, L.J. Gauckler, Identification of the reaction mechanism of the Pt, $O_2(g)$|yttria-stabilized zirconia system, Solid State Ionics 117 (1999) 203.
[55] M. Odgaard, E. Skou, SOFC cathode kinetics investigated by the use of cone shaped electrodes: The effect of polarization and mechanical load, Solid State Ionics 86 (1996) 1217.
[56] T. Iori, T. Hara, Y. Uchimoto, Z. Ogumi, Z. Takehara, Preparation of Perovskite-Type $La_{1-x}Sr_xMnO_3$ Films by Vapor-Phase Processes and Their Electrochemical Properties, J. Electrochem. Soc. 144 (1997) 1362.
[57] E. Siebert, A. Hammouche, M. Kleitz, Impedance spectroscopy analysis of $La_{1-x}Sr_xMnO_3$ – yttria-stabilized zirconia electrode kinetics, Electrochim. Acta 40 (1995) 1753.
[58] S.P. Jiang, Nanoscale and nano-structured electrodes of solid oxide fuel cells by infiltration: Advances and challenges, Int. J. Hydrogen Energy 37 (2012) 449.
[59] R. Barfod, M. Mogensen, T. Klemmensø, A. Hagen, Y.L. Liu, P.V. Hendriksen, Detailed Characterization of Anode-Supported SOFCs by Impedance Spectroscopy, J. Electrochem. Soc. 154 (2007) B371.
[60] N. Bonanos, P. Holtapples, M.J. Jørgensen, Electrochemical evaluation of functionally graded SOFC cathodes, in: Lucerne Fuel Cell Forum, Switzerland, 2002, p. 578.
[61] N. Bonanos, B.C.H. Steele, E.P. Butler, Applications of Impedance Spectroscopy, in: E. Barsoukov, J.R. McDonald (Eds.), Impedance Spectroscopy: Theory, Experiment, and Application, second ed., John Wiley & Sons Inc, Hoboken, NJ, 2005, pp. 258–263.
[62] T. Kenjo, S. Osawa, K. Fujikawa, High temperature air cathodes containing ion conductive oxides, J. Electrochem. Soc. 138 (1991) 349.
[63] T. Kenjo, M. Nishiya, $LaMnO_3$ air cathodes containing ZrO_2 electrolyte for high temperature solid oxide fuel cells, Solid State Ionics 57 (1992) 295.
[64] M. Brown, S. Primdahl, M. Mogensen, Structure/Performance Relations for Ni/Yttria-Stabilized Zirconia Anodes for Solid Oxide Fuel Cells, J. Electrochem. Soc. 147 (2000) 475.
[65] S.H. Jensen, A. Hauch, R. Knibbe, T. Jacobsen, M. Mogensen, Modeling Degradation in SOEC Impedance Spectra, J. Electrochem. Soc. 160 (2013) F244.
[66] J. Nielsen, T. Jacobsen, Three-Phase-Boundary dynamics at metal/YSZ microelectrodes, Solid State Ionics 178 (2008) 1769.
[67] H.K. Song, Y.H. Jung, K.H. Lee, L.H. Dao, Electrochemical impedance spectroscopy of porous electrodes: the effect of pore size distribution, Electrochim. Acta 44 (1999) 3513.
[68] H.K. Song, H.Y. Hwang, K.H. Lee, L.H. Dao, The effect of pore size distribution on the frequency dispersion of porous electrodes, Electrochim. Acta 45 (2000) 2241.
[69] Y. Lu, C. Kreller, S.B. Adler, Measurement and Modeling of the Impedance Characteristics of Porous $La_{1-x}Sr_xCoO_{3-\delta}$, J. Electrochem. Soc. 156 (2009) B513.
[70] K. Eloot, F. Debuyck, M. Moors, A.P. Peteghem, Calculation of the impedance of noncylindrical pores Part I: Introduction of a matrix calculation method, J. Appl. Electrochem. 25 (1995) 326.
[71] K. Eloot, F. Debuyck, M. Moors, A.P. Peteghem, Calculation of the impedance of noncylindrical pores Part II: Experimental verification on pores drilled into stainless steel, J. Appl. Electrochem. 25 (1995) 334.
[72] C. Hitz, A. Lasia, Experimental study and modeling of impedance of the her on porous Ni electrodes, J. Electroanal. Chem. 500 (2001) 213.